J. Magn. Soc. Jpn., **40**, 61-66 (2016)

<Paper>

Fundamental Iron Loss Characteristics of Ring Cores Connected in Series and Parallel under Inverter Excitation

S. Odawara, and K. Fujisaki

Toyota Technological Institute, *Nagoya, Aichi, 468-8511, Japan*

When iron loss characteristics on an inverter excitation are evaluated by using multiple loads connected in series, they indicate lower iron losses compared with using the loads connected in parallel. It indicates that multiple loads should be connected in series to reduce the iron loss when the loads are excited by one inverter. This phenomenon is caused by semiconductor on-voltages changed by the connection method. This conclusion is introduced by an experimental evaluation using three ring cores made of electrical steel sheets (35H300). In addition, to corroborate the experimental results, a numerical analysis is carried out, in which both of characteristics of magnetic hysteresis and semiconductor are taken into account. Analysis results also indicate the same tendency as the experimental results.

Key words: Iron loss, inverter excitation, series-connection, parallel-connection, on-voltage, minor loop

1. Introduction

Utilization rate of electric equipment is increasing in modern society, because of its superior characteristics as controllability, high responsiveness, cleanness and reversibility. In addition, a motor drive system becomes possible to be applied to transportation system as not only automobile but also ship or airplane by power electronics technology.

Since arbitrary frequencies and voltages can be provided in high response by switching operation of inverter, it is possible to control rotation speeds of electrical motors easily. The electrical motors have cores made of magnetic materials such as electrical steel sheets. Therefore, they are excited magnetically with time-harmonics by an inverter for controlling frequencies and voltages. However, the characteristics of electrical steel sheets are determined by a sinusoidal excitation without time-harmonics according to domestic and international standards[1)-2)], and it is usually used for design of the electrical motors.

Many researchers have reported that the carrier harmonics in inverter excitation causes iron loss increase of electrical steel sheet[3)-5)]. In addition, it is revealed in our previous research that the iron loss characteristics are also affected by on-voltages of semiconductor in an inverter circuit: the shape of minor loops is changed by the amplitude of on-voltages and the iron loss is changed by them[6)-9)].

The on-voltages are changed by currents passing the semiconductor. Namely, the on-voltages depend on currents and voltages applied in load such as a motor. Therefore, when multiple loads are excited by using one inverter, the load-currents and the load-voltages are different from the case of single-load due to division of current and voltage. It indicates that the iron loss characteristics are affected by connection method of multiple loads.

A train drive system, in which one inverter drives multiple induction motors connected in parallel, is shown as an example of using multiple loads system[10)]. Moreover, in an electrical motor, the slot winding has an option of series-connection or parallel-connection. These connection methods are selected from a standpoint of controllability[11)-13)] or desired motor characteristics. However, in conventional investigations, iron loss characteristics have not been focused on in the connection methods. Therefore, the connection methods should be investigated from a standpoint of iron loss characteristics to reduce loss on driving system.

Consequently, as a fundamental investigation, the iron loss characteristics are measured by using multiple ring cores made of electrical steel sheets. They are connected in series or in parallel and excited by single-phase PWM (pulse width modulation) inverter. In this study, to obtain the difference by connection method clearly, three ring cores are used for the evaluation. In addition, to corroborate the experimental results, the numerical analysis is also carried out, in which both characteristics of semiconductor and magnetic material are taken into account[14)-16)].

2. Influence of on-voltages on Minor Loops

2.1 Single-load

First, the influence of on-voltages is described by using single-phase inverter shown in Fig. 1 and single-ring shown in Fig. 2(a). The specifications of one ring core are shown in Table I. V_{out} and I_{out} in Fig. 1 are the output-voltage and the output-current of the inverter. V_{on} in Fig. 1 is the on-voltage of semiconductor in the inverter circuit. V_{ring} and I_{ring} in Fig. 2 are the ring-voltage and the ring-current applied to one ring core. The single-phase inverter excitation has two modes: ON-mode and OFF-mode as shown in Fig. 3. The following circuit equations (1) and (2) are obtained from ON-mode and OFF-mode, respectively.

$$V_{dc} = V_s + V_{ring} + V_s, \quad (1)$$

$$0 = V_s + V_{ring} + V_f, \quad (2)$$

where V_s and V_d are the on-voltage of IGBT and diode. Therefore, the ring-voltages V_{ring} of ON-mode and OFF-mode are expressed as the following equations (3) and (4), respectively.

$$V_{ring} = V_{dc} \pm 2V_s, \quad (3)$$

$$V_{ring} = \pm(V_s + V_f). \quad (4)$$

"±" is decided by direction of current flow. For example, when the current flows through voltage source and IGBT 3 and ring and IGBT 2, "–" is selected in equation (3).

Magnetic field intensities H and magnetic flux densities B are calculated by the following equations:

$$H = \frac{N_1 I_{ring}}{l}, \quad (5)$$

$$B = \frac{1}{N_2 S}\int V_{ring}\,dt, \quad (6)$$

where N_1, N_2, l, and S are the primary winding number, the secondary winding number, the average magnetic-path length, and the cross-sectional area of the ring core, respectively. Strictly, the secondary voltage e should be used for calculating B because the voltage drop of the primary coil can be neglected. However, for easy explanation, it is assumed that the primary voltage V_{ring} is the same as the secondary voltage e because N_1 and N_2 are the same.

Fig. 4 shows B-H curve on an inverter excitation. The minor loops are observed and they cause the iron loss increase[6)-8)]. The minor loops are caused by the drop of magnetic flux density ΔB_{off}. ΔB_{off} is caused in OFF-mode of inverter excitation as follow:

$$\Delta B_{off} = \frac{1}{N_2 S}\int_{off} V_{ring}dt = \pm\frac{1}{N_2 S}\int_{off}(V_s + V_f)\,dt. \quad (7)$$

Equation (7) indicates that the minor loops become large when the large on-voltage applies to ring core, and it affects iron losses increase [6)-9)].

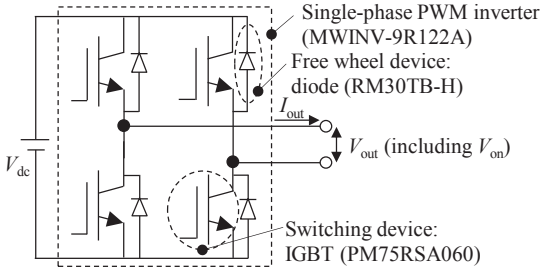

Fig. 1 Single-phase PWM inverter for exciting ring cores.

Table I Specifications of one ring core.

Material	35H300
Outside diameter	127 mm
Inside diameter	102 mm
Height	7 mm
Primary coil winding number	254 turns
Secondary coil winding number	254 turns

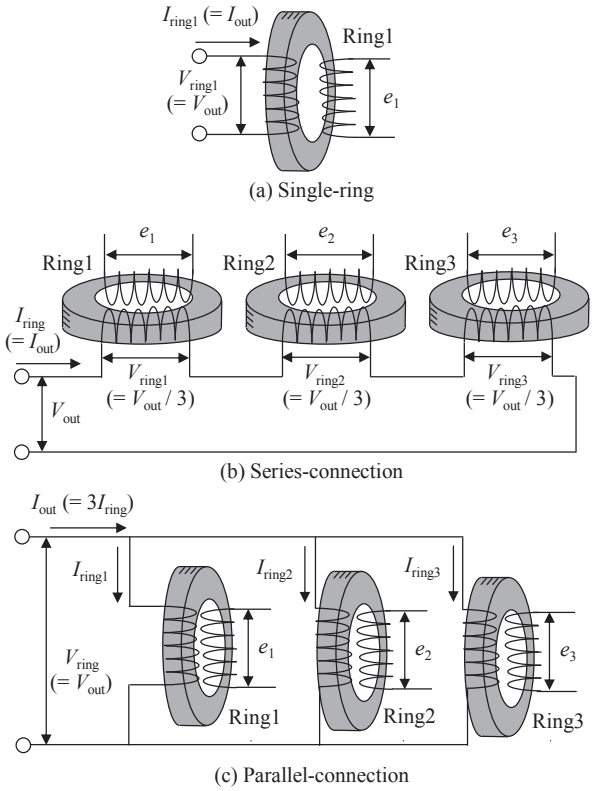

Fig. 2 Connections of ring cores.

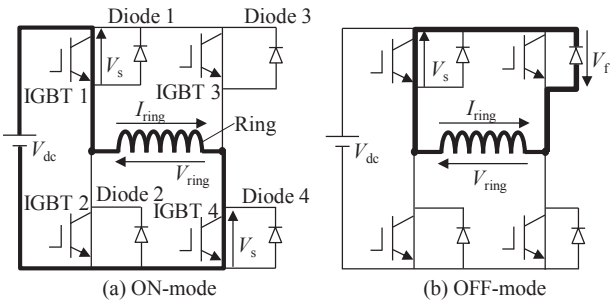

Fig. 3 Current flows in inverter circuit for both modes.

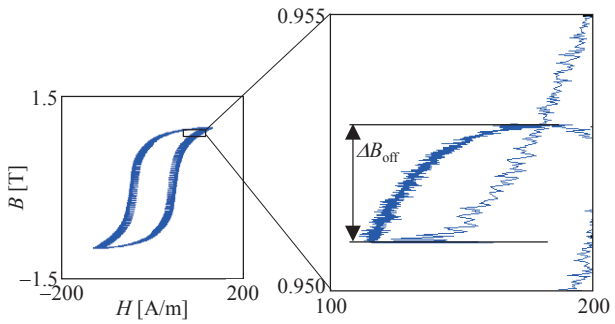

Fig. 4 B-H curve under PWM inverter excitation.

2.2 Three ring cores connected in series or in parallel

In series-connection shown in Fig. 2(b), the ring-voltage V_{ring} becomes a one-third of the output-voltage V_{out}. The ring-current I_{ring} should become the same as the case of single-ring when each ring core is excited under the same excitation conditions as single-ring. Since on-voltages V_{on} depends on I_{ring} (i.e. I_{out}), V_{on} included in V_{out} is also the same as the case of single-ring. Therefore, V_{on} applied to one ring core also becomes a one-third.

On the other hand, in parallel-connection shown in Fig. 2(c), the output-current I_{out} becomes triple of the ring-current I_{ring}. Therefore, V_{on} of parallel-connection becomes large compared with that of single-ring, because I_{out} flowing in the semiconductor is three times larger than that of single-ring. It causes changing the operating point in current-voltage (I-V) characteristics of semiconductor.

Thus, V_{on} applied to one ring core in series-connection becomes smaller than parallel-connection. It is expected that the iron losses in series-connection will become smaller than that in parallel-connection.

3. Experimental Investigation

3.1 Method for measurements

The three ring cores connected in series or in parallel are excited by single-phase inverter shown in Fig. 1 under the following conditions: fundamental frequency f_0 is 50 Hz, modulation index m is 0.6, and carrier frequency f_c is changed from 1 kHz to 20 kHz. The applied DC voltage V_{dc} is set so that the maximum magnetic flux density B_{max} becomes 1 T in each ring core.

3.2 On-voltages on each connection

First, on-voltage V_{on} included in ring-voltage V_{ring} is evaluated to confirm an influence by difference of connection method. Fig. 5 shows output-current I_{out} and V_{ring1} waveforms of ring 1 on f_c = 10 kHz and the enlargement near the maximum I_{out}. V_{on} emerges as voltage protrusion from zero on OFF-mode as shown in Fig. 5(b).

In Fig. 5, it is confirmed that the on-voltages are changed by the series-connection and the parallel-connection. On the series-connection waveform shown in Fig. 5 (c), the on-voltage becomes about a one-third of on-voltage on single-ring due to voltage dividing.

On the other hand, the on-voltage on parallel-connection shown in Fig. 6 (d) is a little larger than that on single-ring, because I_{out} flowing in semiconductor becomes about three times larger than single-ring. It causes changing the operating point on I-V characteristics in semiconductor. These phenomena are described in detail in next analytical investigation chapter.

The experimental results indicate the phenomena according to the theory mentioned in section 2-2. Therefore, it is confirmed from the experiment that the on-voltages characteristics are changed by the series-connection and the parallel-connection.

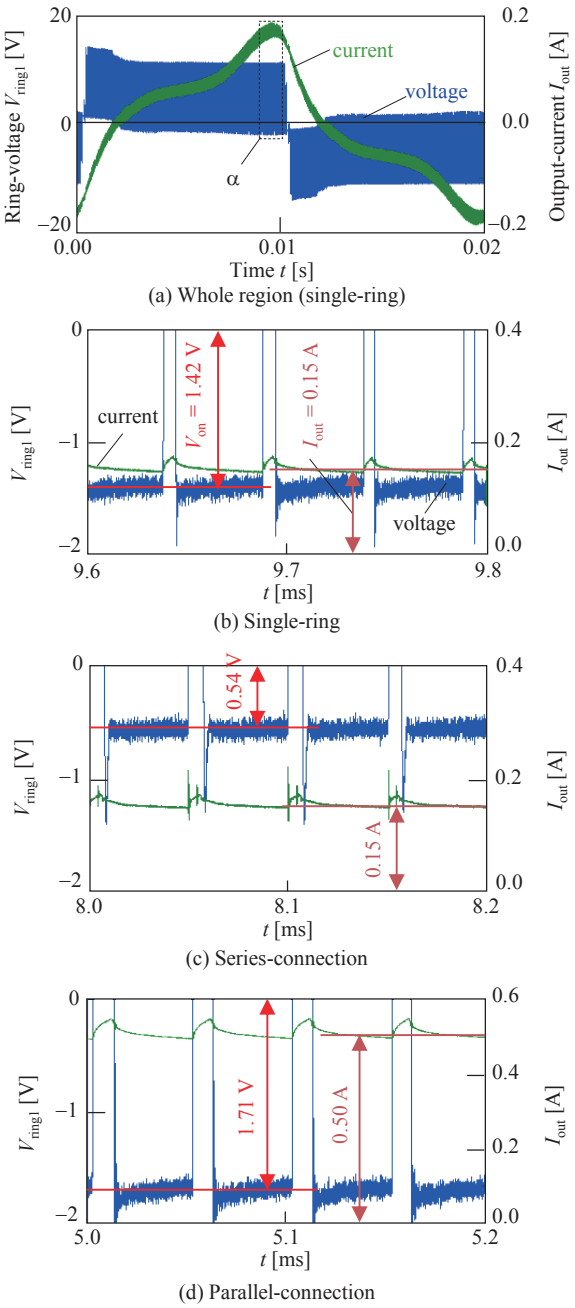

Fig. 5 Measured on-voltages from each connection (f_c = 10 kHz).

3.3 *B*-*H* curves

B-*H* curves are depicted from obtained *B* and *H* in the series-connection and the parallel-connection. Fig. 6 shows the measured *B*-*H* curves in ring 1 obtained from both connections on f_c = 10 kHz. It also shows minor loops near the maximum flux density. The minor loop of series-connection is smaller than that of parallel-connection, because the on-voltage of series-connection is small. The minor loop leads the iron loss increase because the iron loss is proportional to surface integral of *B*-*H* hysteresis curve and the surface integral is performed in addition on the minor loops. Therefore, it is expected that the iron loss becomes small in series-connection.

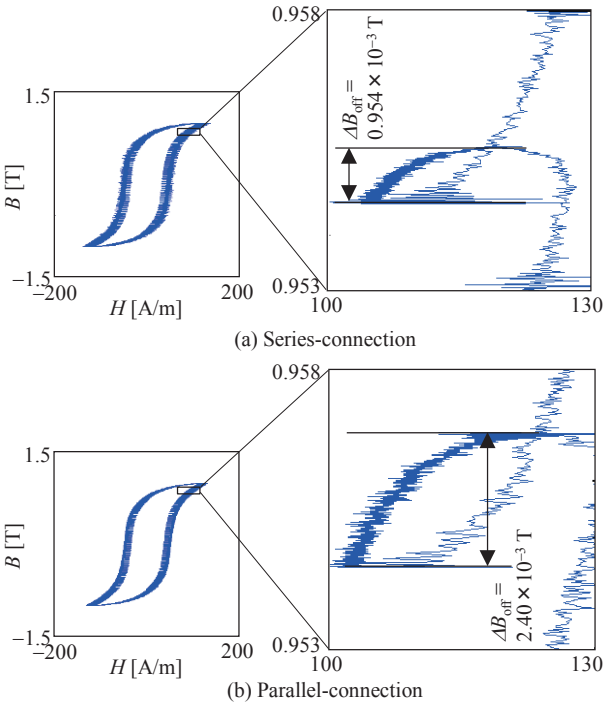

Fig. 6 Measured B-H curves in ring 1 (f_c = 10 kHz).

3.4 Iron loss characteristics

Finally, the iron loss characteristics are evaluated in both connections. The iron loss is calculated by the following equation (8). In the measurement, it is difficult to set the maximum flux density B_{max} to 1 T strictly. Therefore, a normalization of iron loss on just B_{max} = 1 T is performed by using the following equation (9). In equation (9), the iron loss is assumed to be proportional to the square of magnetic flux density.

$$W_{fe} = \frac{f_o}{\rho}\int HdB, \tag{8}$$

$$W_{fe}^{*} = W_{fe} \times 1^2 / B_{max}^2, \tag{9}$$

where ρ is the density of electrical steel sheet (= 7650 kg/m^3) and superscript (*) means the normalized value.

Table II shows the iron losses obtained from each connection on f_c = 10 kHz. In Table II, it is indicated that there is no dispersion of three rings characteristics because the iron losses are the same as each other. The iron losses of series-connection are smaller than that of parallel-connection. The total iron loss of parallel-connection is about 3.8 % larger than series-connection.

To confirm the phenomenon, the iron losses are obtained by changing the carrier frequencies. Fig. 7 shows the carrier frequency characteristics of total iron loss on each connection. In each carrier frequency, the iron losses from series-connection are smaller than that from parallel-connection. The minimum peak indicated in Fig. 8 is caused by dead-time effect of inverter excitation. The dead-time makes additional applied voltage require in higher carrier frequency[17]. It makes additional current (i.e. additional H) and makes the loss increased.

Table II Iron losses on each connection (f_c = 10 kHz).

W_{fe}^{*} [W/kg]	Series connection	Parallel connection
Ring 1	1.14	1.18
Ring 2	1.14	1.19
Ring 3	1.14	1.18
Total	3.42	3.55

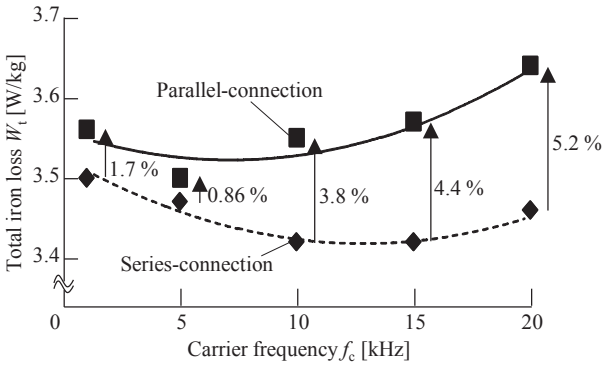

Fig. 7 Carrier frequency characteristics of total iron loss obtained from experiment.

4. Analytical Investigation

4.1 Method for analysis

A numerical analysis[15)-16)] is carried out to corroborate the phenomena obtained from the experiment. The numerical analysis can take into account both of semiconductor characteristics and magnetic hysteresis characteristics. The analysis is performed according to flowchart shown in Fig. 8[16)].

When the circuit analysis is carried out in process (v), on-voltages are calculated by using I-V characteristics. Fig. 9 shows the I-V characteristics of semiconductors used for this analysis. The operating points of the series-connection and the parallel-connection, which are mentioned in section 3-2, are also shown in Fig. 9. In Fig. 9, an approximation according to a quadratic expression is performed on region less than the current of 1 A, because it cannot be obtained from datasheets. V_{CE} and V_F correspond to the on-voltages of the IGBT and the diode, respectively.

When the magnetic analysis is carried out in process (iii), Play model[18)-19)] and Cauer's equivalent circuit[20)-21)] shown in Fig. 10 are used for considering magnetic hysteresis. The magnetic field intensity H is calculated by inputting the magnetic flux density B obtained from generated output-voltage in circuit analysis. In Cauer's circuit, v, i, L, and R_E correspond to dB/dt, H, the permeability, and the classical eddy-current loss, respectively. By solving the circuit equation, the following equations are obtained.

$$H^k(B^k) = H_1^k + H_2^k + H_3^k, \tag{10}$$

$$R_E = \frac{12}{\kappa\sigma d^2}, \tag{11}$$

$$H_2^k = C_1 H_3^k + H_2^{k-1}, \quad (12)$$

$$H_3^k = \frac{1}{C_2}\{3(B^k - B^{k-1}) - 3R\Delta t H_2^{k-1}\}, \quad (13)$$

$$C_1 = \frac{35}{3L'} R\Delta t, \quad (14)$$

$$C_2 = R\Delta t(3C_1 + 10) \quad (15)$$

where σ is the electric conductivity (= 1.92*10^6 S/m), d is the thickness of electrical steel sheets (= 0.35 mm). κ is the anomaly factor and it is set to 2 according to Ref. (16). L' is linear inductance and it is set to 1.6 mH according to Ref. (16). The DC magnetic properties $H_{DC}(B)$ is obtained by scalar play model[18)-19)].

In this numerical analysis, influences of dead-time and rise time of the semiconductor are neglected for simplicity.

4.2 Analysis results

Fig. 10 shows analyzed on-voltages corresponding to Fig. 5. The on-voltage values is the almost same as experimental results shown in Fig. 5. Fig. 12 shows the analyzed hysteresis curves on the series-connection and the parallel-connection. The analysis results express not only the major loop but also the difference of minor loops sizes obtained from measurement shown in Fig. 6.

Fig. 13 shows the carrier frequency characteristics on total iron loss corresponding to Fig. 7. The analysis results indicate the same tendency as experimental results: the iron loss obtained from parallel-connection is larger than that from series-connection on each carrier frequency.

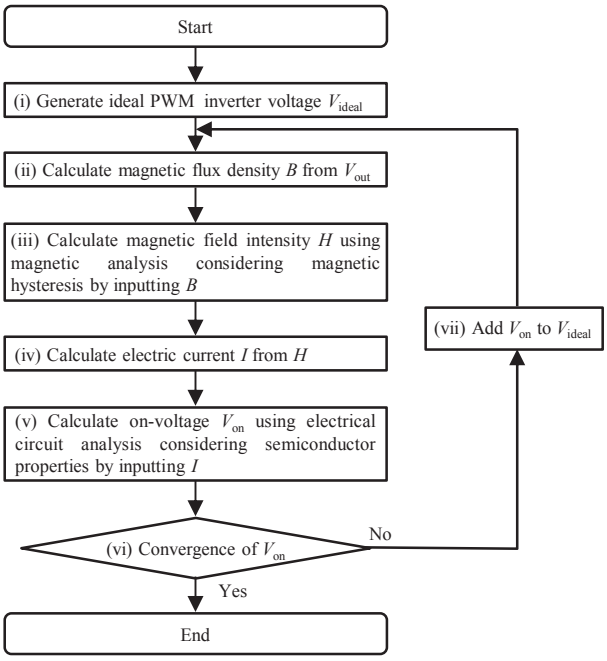

Fig.8 Flowchart of numerical calculation taking into account semiconductor characteristics and magnetic material[16)].

In this analysis, the dead-time effect is neglected for simplicity. Therefore, the minimum peak mentioned in Fig. 7 is not observed. Moreover, the analyzed difference of the parallel-connection and the series-connection is smaller than the experimental results. It is caused by dead-time effects. Dead-time makes additional current require on higher carrier frequency. Therefore, since additional current also becomes three times in parallel-connection, V_{on} is easy to be affected by the additional current. It causes the difference of analysis and experiment.

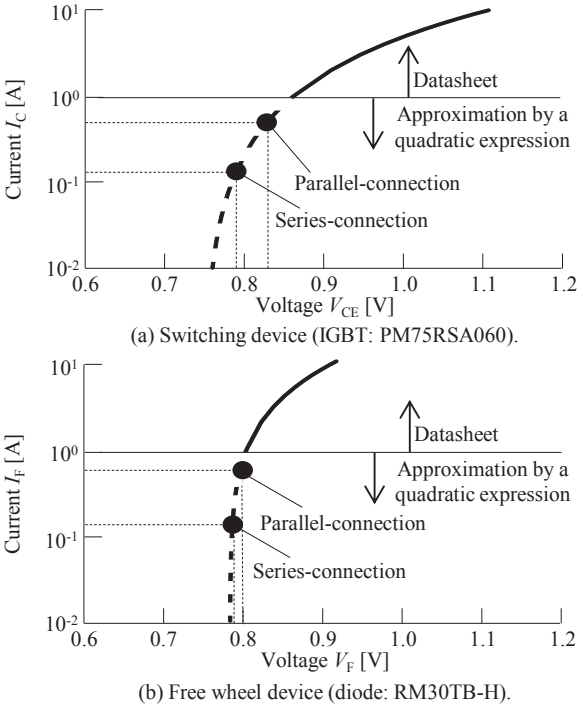

Fig. 9 I-V characteristics of power semiconductors and operating points on both connections.

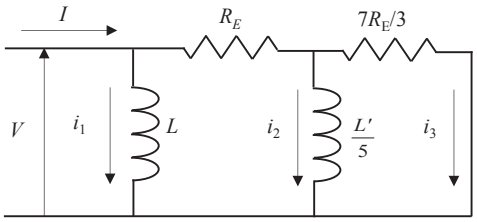

Fig. 10 Cauer's equivalent circuit to consider magnetic hysteresis characteristics.

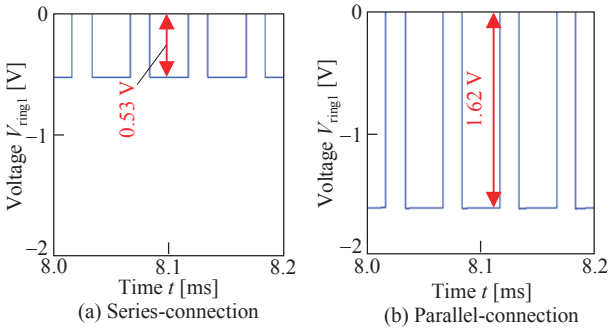

Fig. 11 Analyzed on-voltages from each connection (f_c = 10 kHz).

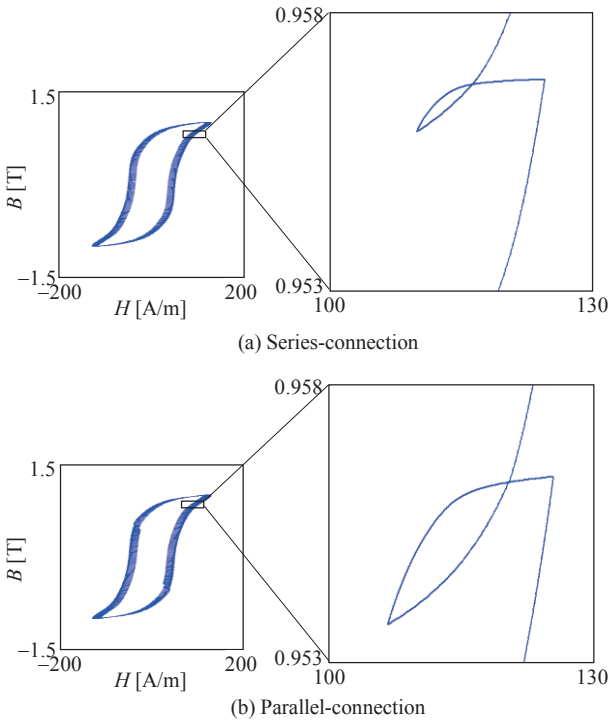

Fig. 12 Analyzed B-H curves in ring 1 (f_c = 10 kHz).

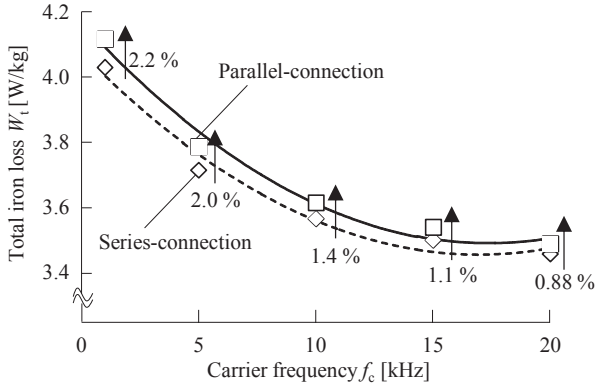

Fig. 13 Carrier frequency characteristics of total iron loss obtained from numerical analysis.

5. Conclusion

The influence of series-connection and parallel-connection is evaluated from the standpoint of iron loss characteristics. The on-voltage, the B-H curve, and the iron loss are obtained by measurement using three ring cores. Obtained results are shown as follows.

1) On-voltages of each ring core on series-connection become three times smaller than that on parallel-connection, because the voltage dividing of on-voltage is caused by series-connection.
2) Since on-voltage on series-connection is small, minor loops in magnetic hysteresis which is led by the on-voltage becomes smaller than parallel-connection.
3) Since minor loops of series-connection is small, iron loss on series- connection is smaller than parallel-connection.
4) These results are also corroborated by the numerical analysis taking into account both of the magnetic hysteresis property and the semiconductor property.

According to these results, in order to reduce the iron losses, multiple loads should be connected in series when they are driven by one inverter.

Acknowledgements Part of this research was supported by Ministry of Education, Culture, Sports, Science and Technology (MEXT) program in Japan for private universities.

References

1) International Electrotechnical Commission, 60404-3, Second edition, 1992.
2) Japanese Industrial Standard, C2556, 1996.
3) A. Boglietti, P. Ferraris, M. Lazzari, and F. Profumo: *IEEE Trans. Magn.*, vol. **27**, no. 6, pp.5334-5336, 1991.
4) M. Kawabe, T. Nomiyama, A. Shiozaki, H. Kaihara, N. Takahashi, M. Nakano: *IEEE Trans. Magn.*, vol. **48**, no. 11, pp. 3458–3461, 2012.
5) H. Matsumori, T. Shimizu, K. Takano, and H Ishii: *Energy Conversion Congress and Exposition (ECCE)*, 2012.
6) K. Fujisaki, and S. Liu: *Journal of Applied Physics*, **115**, 17A321, 2014.
7) D. Kayamori, K. Fujisaki: *IEEE Power Electronics and Drive Systems (PEDS)*, 9034, 2013.
8) S. Odawara, D. Kayamori, and K. Fujisaki: *IEEJ Trans. Industry Applications,* vol.**134**, no.7, pp. 649-655, 2014, (in Japanese).
9) S. Odawara, D. Kayamori, and K. Fujisaki: *IEEJ Trans. Fundamentals and Materials*, vol.**135**, no.7, pp. 385-390, 2015, (in Japanese).
10) T. Hasebe, and H. Yamamoto: *Toshiba review*, vol. **61**, no. 9, 2006 (in Japanese).
11) T. Nagano, Y. Nakajima, Y. Noge, and J. Itoh: *IEEJ Industry Applications Society Conference,* L2177B, 2012 (in Japanese).
12) K. Matsuse, H. Kawai, Y. Kouno, and J. Oikawa: *IEEE Trans. Industry Applications,* vol. **40**, no. 1, pp. 153-161, 2004.
13) N. Urasaki, T. Senjyu, and K. Uezato: *IEEE Trans. Energy Conversion,* vol. **19**, no. 2, pp. 265-270, 2004.
14) S. Odawara, K. Fujisaki, and F. Ikeda: *IEEE Trans. Magn.*, vol. **50**, no. 11, article #: 7201004, 2014.
15) S. Odawara, K. Fujisaki, and T. Matsuo: *Energy Conversion Congress and Exposition (ECCE)*, P2105, 2014.
16) S. Odawara, K.Fujisaki, T. Matsuo, and Y. Shindo: *IEEJ Trans. Industry Applications,* vol. **135**, no. 12, 2015 (in Japanese).
17) T. Tanaka, S. Koga, R. Kogi, S. Odawara, and K. Fujisaki: *IEEJ Trans. Industry Applications,* vol. **136**, no. 2, 2015 (in Japanese) (in press).
18) S. Bobbio, G. Miano, C. Serpico and C. Visone: *IEEE Trans. Magn.*, vol. **33**, no. 6, pp. 4417-4426, 1997.
19) T. Matsuo and M. Shimasaki: *IEEE Trans. Magn.*, vol. **41**, no. 10, pp. 3112-3114, 2005.
20) J. H. Krah : *IEEE Trans. Magn*, vol. **41**, no. 5, pp. 1444-1447, 2005.
21) Y. Shindo, O. Noro: *IEEJ Trans. FM*, vol.**134**, no.4, pp. 173- 181, (2014).

Received Nov. 05, 2015; Revised Dec. 30, 2015; Accepted Jan. 25, 2016